euspen's 26th International Conference & Exhibition, Krakow, PL, June 2026

www.euspen.eu

Ultra-precision machining of superhydrophobic surfaces with re-entrant microstructures

Douwei Liu, Wenbin Zhong*, Wenhan Zeng, Xiangqian Jiang

EPSRC Future Metrology Hub, Centre for Precision Technologies, School of Computing and Engineering, University of Huddersfield, Huddersfield, HD1 3DH, UK

*w.zhong@hud.ac.uk

Abstract

Superhydrophobic surfaces have attracted extensive attention due to their outstanding water-repellent properties and promising applications in self-cleaning, corrosion resistance, anti-icing, drag reduction, and microfluidics. Conventionally, superhydrophobicity is achieved through the synergistic effect of surface micro/nanostructures and low-surface-energy chemical modifications. However, chemical surface treatments often suffer from limited durability, poor environmental stability, and complex fabrication processes, which restrict their long-term engineering applications. In this study, a superhydrophobic surface fabrication strategy based on ultra-precision machining is proposed, enabling the direct machining of re-entrant microstructures on a brass substrate. Benefiting from the high precision, material versatility, and geometric flexibility of ultra-precision machining, well-defined re-entrant microstructures were successfully fabricated. Wetting characterization reveals that the fabricated surface can stably maintain the Cassie–Baxter state without any chemical surface modification, exhibiting an apparent water contact angle of approximately 133°, a sliding angle of about 28°, and remarkably low droplet adhesion. These results demonstrate that ultra-precision machining provides a feasible and scalable approach for the fabrication of chemically unmodified superhydrophobic surfaces, offering new opportunities for the engineering application of durable functional surfaces.

Re-entrant; Ultra-precision machining; Superhydrophobic surfaces

1. Introduction

Inspired by natural surfaces such as lotus leaves and insect cuticles, superhydrophobic surfaces have attracted extensive attention due to their outstanding water-repellent properties and broad application potential in self-cleaning, corrosion resistance, anti-icing, drag reduction, and microfluidics. Superhydrophobicity is generally attributed to the combined effect of surface micro/nanostructures and low-surface-energy chemical modifications. Conventional strategies typically rely on constructing hierarchical structures followed by chemical modification with agents such as fluoroalkyl silanes to reduce surface energy [1]. However, these chemical treatments often suffer from poor durability, environmental instability, and complex processing, limiting their long-term practical applications. Consequently, achieving superhydrophobicity without chemical surface modification has become an important research direction.

Re-entrant microstructures, inspired by the cuticular morphology of springtails, have been demonstrated to enable stable superhydrophobicity by sustaining a Cassie–Baxter wetting state without chemical modification. In such structures, trapped air pockets support liquid droplets and reduce the solid–liquid contact fraction, thereby enhancing water repellence [2],[3]. Nevertheless, the fabrication of re-entrant structures generally depends on complex manufacturing techniques, such as photolithography, etching, or two-photon polymerization, which are constrained by material compatibility, feature size, fabrication efficiency, and process complexity [4].

Ultra-precision machining offers notable advantages for microstructure fabrication, including material versatility, high efficiency, and excellent geometric flexibility through tool path control [5]. However, the fabrication of re-entrant structures via ultra-precision machining remains challenging due to unavoidable tool interference arising from geometric constraints, which has limited its application to non–re-entrant microstructures. As a result, studies on machining-based fabrication of chemically unmodified superhydrophobic re-entrant structures are still scarce.

In this work, a novel superhydrophobic surface fabrication method based on ultra-precision machining is proposed. Re-entrant microstructures are designed using classical wetting theory and mechanical equilibrium analysis and then fabricated on an ultra-precision turning platform with on-machine measurement and optimized tool path planning. The wetting performance is evaluated experimentally and through multiphase flow modelling.

2. Method

2.1. Wetting theory and design of re-entrant structures

To stabilize the Cassie–Baxter state on intrinsically hydrophilic surfaces without altering surface chemistry, the introduction of re-entrant microstructures with overhanging features is considered an effective strategy. Re-entrant structures significantly increase the energy barrier that must be overcome for the transition from the Cassie–Baxter state to the Wenzel state, thereby mechanically suppressing liquid penetration into the microstructures.

From a mechanical equilibrium perspective, the stability of a droplet in the Cassie–Baxter state on re-entrant structures depends on whether the capillary pressure generated by the gas–liquid interface can counterbalance the hydrostatic pressure of the droplet, as shown in Figure 1. For a curved gas–liquid interface formed within a re-entrant cavity, the pressure balance across the interface can be expressed as Eq 1, where $P_g = \rho g h$ represents the hydrostatic pressure of the droplet, with ρ being the liquid density, g the gravitational acceleration, and h the droplet height.

$$P_{l2} = P_{l1} + P_g \quad (1)$$

P_{l1} and P_{l2} denote the Laplace pressures at the external droplet contour interface and at the gas–liquid interface inside the re-entrant structure, respectively, which can be expressed as Eq.2, where γ is the liquid–gas interfacial tension, b_1 is the radius of curvature at the apex of the droplet's external contour, and b_2 is the radius of curvature of the curved gas–liquid interface formed between adjacent microstructures.

$$P_{l1} = \frac{2\gamma}{b_1}, P_{l2} = \frac{2\gamma}{b_2} \quad (2)$$

For simplicity, the droplet shape is approximated as a spherical cap, which facilitates the estimation of the curvature radii and droplet height.

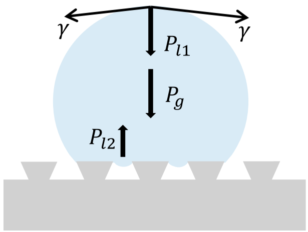

Figure 1. The force balance model of the re-entrant structured surface.

2.2. Ultra-precision machining of re-entrant structured surface

The ultra-precision machining tool, Moore Nanotech 650 FGV2 is used here, and the machining setup is illustrated in Figure 2 (a). The sharp edge single-point diamond cutting tool with the included angle θ_t is used here, as shown in Figure 2 (b). Unlike conventional machining configurations in which the tool tip axis is perpendicular to the workpiece surface, the tool tip is intentionally tilted in this study to enable the machining of re-entrant structures, as shown in Figure 3(a).

After the cutting tool is tilted by angle $\alpha_{r,l}$, its position relative to the initial workpiece coordinate system undergoes corresponding translational displacements $\Delta x_{r,l}$ and $\Delta z_{r,l}$. These displacements are determined by the installation position of the tool tip relative to the machine tool rotational center, characterized by the parameters γ and r. Here, γ denotes the angle between the line connecting the tool tip and the B-axis rotational centre of the machine and the machine z-axis, while r represents the distance from the tool tip to the rotational center.

It can be inferred that the positional offsets are uniquely determined by the rotation angle and the installation parameters. Therefore, accurate calibration of the tool tip installation position is critical for the fabrication of re-entrant structures. In this study, a trial-cutting method is employed to determine the actual installation position of the tool tip point relative to the machine tool. According to the geometric relationship, when the tool tip is rotated by an angle α, the corresponding displacements of the tool tip point are Δx and Δz, which satisfy the following relationships, Eq 3.

$$\begin{cases} \Delta x = 2 * r * \sin\left(\frac{\alpha}{2}\right) * \sin\left(\gamma + \frac{\pi - \alpha}{2}\right) \\ \Delta z = 2 * r * \sin\left(\frac{\alpha}{2}\right) * \cos\left(\gamma + \frac{\pi - \alpha}{2}\right) \end{cases} \quad (3)$$

Scratches are generated on the workpiece surface using the cutting tool, and the displacement Δx and Δz of the scratches is measured by a chromatic confocal probe [6]. Based on these measured values, the actual installation offsets γ, r of the tool tip relative to the machine tool can be calculated according to Eq 3.

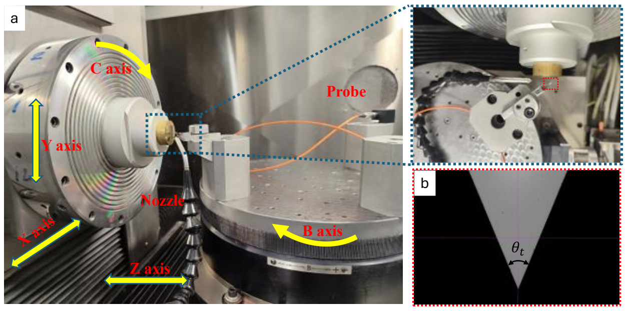

Figure 2. Ultra-precision machining of re-entrant structured surface. (a) machining set-up for the diamond tool and (b) the sharp edge single-point diamond cutting tool used in the machining under tool-setter.

As shown in Figure 3, after tilting, the angle between the tool axis and the Z-axis of the workpiece coordinate system is denoted as α. Accordingly, the re-entrant angle of the machined structure, θ, satisfies the following relationship, Eq 4.

$$\theta = 90^{\circ} - \alpha + \frac{\theta_t}{2} \quad (4)$$

It can be inferred from this equation that the re-entrant angle θ of the machined structure is jointly determined by the tool included angle θ_t and the tilting angle α. In this study, to fabricate microgrooves with a re-entrant angle of 60°, a diamond tool with an included angle of 45° was employed, corresponding to a tool tilting angle of 52.5°.

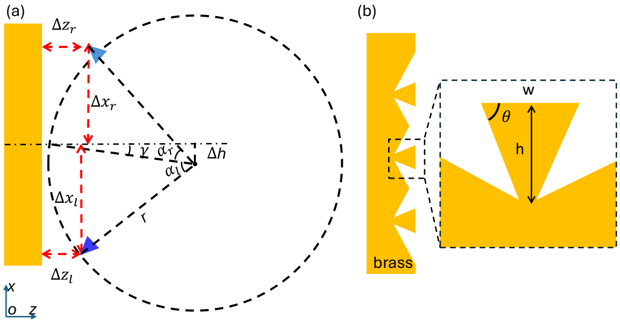

Figure 3. The schematic diagram shows the ultraprecision machining of re-entrant structures with (a) the moving of cutting tool under view of xoz plane of machine tool and (b) the re-entrant structures generated by ultra-precision machining.

After the generation of a single re-entrant structure, the cutting tool is translated along the z-direction to generate an array of re-entrant structures. According to the Eq 1 and Eq 2, the width $w = 25\mu m$ height $h = 15\mu m$ and space with 35 µm of the re-entrant structures showing in Figure 3 are controlled by the tool translation distance. In addition, because the intersection between adjacent tool paths cannot completely remove the substrate material, residual structures are formed between adjacent re-entrant features, as illustrated in Figure 3. In the present study, the spacing between adjacent re-entrant structures is insufficient to allow the liquid droplet to penetrate the microstructure gaps [7]. Moreover, the sagging height of the droplet between adjacent re-entrant structures is not large enough to contact the residual structures [7]. Therefore, the residual height does not affect the wetting behaviour of the droplet and can be neglected in this study.

2.3 Simulation of droplet wetting on re-entrant structured surface

To investigate the wetting behaviour of droplets on re-entrant structured surfaces and the dynamic evolution of the gas–liquid interface, a multiphase flow numerical model based on the phase-field method was established. The wetting process of a droplet on microstructure surfaces was systematically analysed. The fluid motion of both the gas and liquid phases was governed by the Navier–Stokes equations under laminar flow conditions, while the Cahn–Hilliard equation was employed to solve the phase-field variable, enabling continuous tracking and evolution of the gas–liquid interface.

Since the initial velocity of the droplet during the wetting process can be regarded as zero, and both the gas and liquid phases can be approximated as Newtonian fluids, the characteristic Reynolds number of the system is relatively low. Therefore, a laminar flow model was adopted. The continuity equation is given by Eq 5.

$$\rho\nabla\cdot\mathbf{u}=0 \tag{5}$$

To accurately capture the evolution of the gas–liquid interface within the phase-field framework, the Cahn–Hilliard model was employed. The governing equations of the phase-field model are expressed as Eq 6, where ψ is the chemical potential, γ is the phase-field mobility parameter, ε represents the characteristic thickness of the gas–liquid interface, and λ is the mixing energy density parameter, which is closely related to the interfacial tension.

$$\begin{cases}\frac{\partial\phi}{\partial t}+\nabla\cdot(\mathbf{u}\phi)=\nabla\cdot\left(\gamma\frac{\lambda}{\varepsilon^2}\nabla\psi\right)\\ \psi=-\nabla\cdot(\varepsilon^2\nabla\phi)+(\phi^2-1)\phi+\frac{\varepsilon^2}{\lambda}\frac{\partial f}{\partial\phi}\end{cases} \tag{6}$$

To ensure numerical stability while accurately representing interfacial tension effects and avoiding nonphysical interface diffusion, the interface thickness and mobility parameters were selected following the parameterization method proposed by Bellussi *et al*[8].

The mixing energy density parameter λ can be expressed as Eq.7, where σ denotes the gas–liquid interfacial tension.

$$\lambda=\frac{3\varepsilon\sigma}{2\sqrt{2}} \tag{7}$$

The boundary conditions of the numerical model were defined as follows: the left and right boundaries as well as the top boundary of the computational domain were set as flow outlets with an outlet pressure of 0 Pa; the re-entrant structured surface was defined as a wetted wall with a no-slip boundary condition applied. The intrinsic contact angle of the wall was set to 71°, which was obtained from experimental contact angle measurements on the brass substrate and was used to define the wetting boundary condition in the phase-field model.

With the above model configuration, the wetting behavior of droplets on re-entrant microstructured surfaces and the stability of the gas–liquid interface can be quantitatively analyzed. All numerical simulations of the wetting model were performed using the commercial finite element software COMSOL Multiphysics 6.3.

The simulation results were shown in Figure 4. During the spreading process, the droplet remains suspended above the structured surface without penetrating the microcavities. Owing to the symmetric configuration adopted in the numerical simulations, the contact angles on the left and right sides of the droplet are identical.

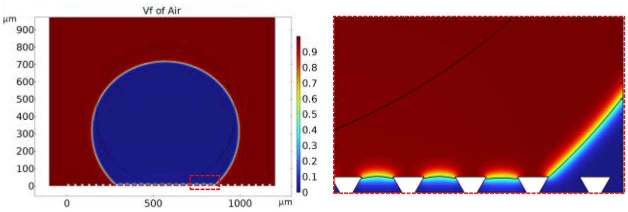

Figure 4. The simulation of droplet on the re-entrant surface.

3. Results and discussion

3.1 Calibration of tool position

Single-sided scratching experiments were conducted with tool tilting angles of 30°and 45°, respectively. Figure 5 presents the on-machine measurement results of the scratches, from which the corresponding displacement values were calculated, as summarized in Table 1.

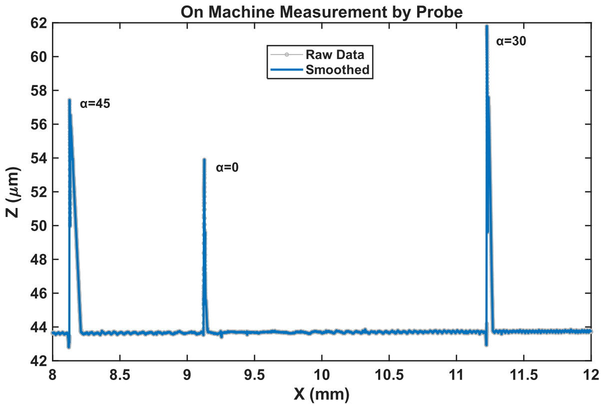

Figure 5. On machine measurement of cutting scratches under different tilting angles.

The results obtained with a tool tilting angle of 30°were used for the calculation. According to the derived equations, the corresponding values of $\gamma=2.887°$and $r=180.402$ mm were obtained. Under the same installation parameters, the differences between the theoretical and experimentally measured displacements in the x and z directions for the 45° tilting case were calculated with $\mathrm{Error_z}=2$ μm and $\mathrm{Error_x}=8$ μm, respectively.

These errors may originate from inaccuracies in probe-based measurements of the tool tip position relative to the spindle centre in the untitled configuration. In addition, plastic recovery of the material and wear of the tool tip make it difficult to obtain a perfectly symmetric groove profile, which further affects the measurement of the tool tip position relative to the initial cutting depth. To compensate for the tool tip positioning errors, an additional trial-cutting compensation method was employed during the actual machining process.

Table 1 On machine measurement of cutting tool installation

α(deg)	Δz(mm)	Δx(mm)
30	19.595	91.304
45	46.346	130.063

3.2 The surface characteristics

The machined re-entrant structures were characterized using an Alicona G5 optical measurement system. The surface morphology of the microstructures is shown in the Figure 6. Under the tilted-tool machining strategy, groove structures with a width of 25.1 μm and a space of 35.7 μm were successfully generated. Consistent with the machining principle, material residues formed by the intersection of adjacent tool paths were observed between neighbouring microstructures. Due to the occlusion caused by the re-entrant geometry, it is difficult to directly measure the re-entrant angle. In addition, SEM characterization can reveal the re-entrant angle by measuring the cross-sectional profile. However, the preparation of cross-sectional samples inevitably causes damage to the re-entrant structures, which are particularly fragile at their root regions. Therefore, in this research, the residual material was used as an indirect indicator for estimating the inclination angle of the re-entrant structures. As shown in Figure 6, the average inclination angle θ of the residual region is calculated to be 15.7°. As the included angle of diamond tool θ_t is 45°, the re-entrant angle of the fabricated structures is determined to be 60.7°, demonstrating that the fabricated structure is in excellent agreement with the designed re-entrant angle of 60°.

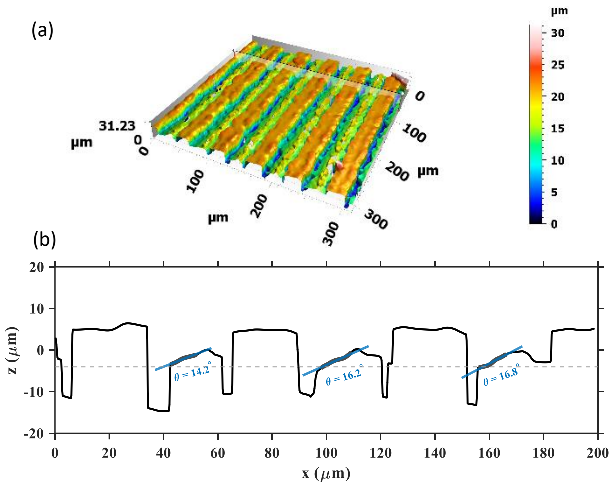

Figure 6. The measurement of generated surfaces with re-entrant structures with (a) showing the 3D of the re-entrant structured surfaces and (b) showing the profile of the re-entrant structures, here *θ* is the inclination angle of the residual region.

3.3 The wetting result on re-entrant structured surfaces

The wetting behaviour of the fabricated re-entrant structures was characterized using a self-built contact angle measurement system. Deionized water was used as the test liquid, and droplets were dispensed through a needle with an inner diameter of 0.25 mm. The droplet volume was controlled at 4 µL and gently deposited onto the surface. Each droplet was measured four times to reduce experimental uncertainty, and the average value was reported.

As shown in Figure 7, The measured contact angle on the left side of the droplet was 135.7°, while that on the right side was 130.2°, resulting in an average contact angle of 132.9°. The discrepancy between the left and right contact angles arises from tool tilting and machining errors, which lead to slight asymmetry between the two sides of the grooves rather than a perfectly symmetric structure.

Based on the measured structural dimensions, the apparent contact angle of the droplet was calculated using the Cassie–Baxter model and the Wenzel model, respectively. Comparison with the experimentally measured contact angle indicates that the droplet resides in the Cassie–Baxter state rather than the Wenzel state.

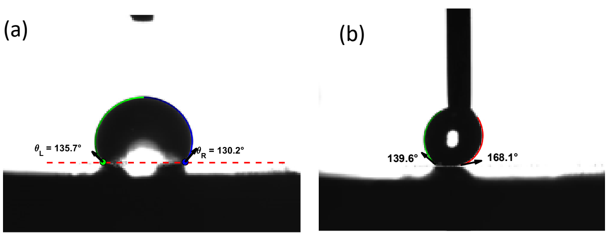

Figure 7. The wetting experiment of droplet on the re-entrant surface with (a) the contact angle and (b) the contact angle hysteresis.

To further verify the wetting state of the droplet on the fabricated re-entrant structured surface, contact angle hysteresis measurements were performed. The results show that the advancing and receding contact angles are 139.6°and 168.1°, respectively, yielding a contact angle hysteresis of 28.5°. The relatively low contact angle hysteresis further indicates the low adhesion of the droplet on the machined re-entrant structures, confirming that the droplet resides in the Cassie–Baxter state. In addition, during droplet rolling experiments, trapped air beneath the droplet within the re-entrant structures can be directly observed, providing further evidence of the Cassie–Baxter wetting state.

4. Conclusion

This study investigated an ultra-precision machining approach for fabricating re-entrant structured surfaces and proposed a tilted-tool-axis machining strategy that enables high-precision fabrication of re-entrant microstructures on a brass substrate. This method effectively circumvents the geometric interference limitations inherent in conventional tool path planning and demonstrates the feasibility and machining flexibility of ultra-precision subtractive manufacturing for complex re-entrant structures.

By wetting experiments the results demonstrate that without any surface chemical modification, the fabricated re-entrant structures can stably maintain the Cassie–Baxter wetting state, exhibiting an apparent contact angle of 132°, a sliding angle of about 28°, and low droplet adhesion. The experiment shows good agreement with the simulation, further elucidating the role of trapped air cavities within the re-entrant structures in supporting the droplet and stabilizing the wetting state.

This work provides a new technological pathway for the design and fabrication of chemically-free superhydrophobic structures and expands the application scope of ultra-precision machining in functional surface engineering. Future studies may focus on optimizing microstructural geometric parameters, extending material applicability, and evaluating the durability of the structures under complex service conditions to further enhance their wetting performance and engineering application potential.

References

[1] Lian, Z., Zhou, J., Ren, W., Chen, F., Xu, J., Tian, Y., Yu, H., 2024. Recent progress in bio-inspired macrostructure array materials with special wettability—from surface engineering to functional applications. *Int. J. Extrem. Manuf.* **6**, 2631-8644.

[2] Cao, L., Hu, H.-H., Gao, D., 2007. Design and Fabrication of Micro-textures for Inducing a Superhydrophobic Behavior on Hydrophilic Materials. *Langmuir.* **23**, 4310–4314.

[3] Wang, B., Chen, J., Kowall, C., Li, L., 2020. 3D-Printed Repeating Re-Entrant Topography to Achieve On-Demand Wettability and Separation. *ACS Appl. Mater. Interfaces* **12**, 35725–35730.

[4] Liu, T. "Leo", Kim, C.-J. "CJ," 2014. Turning a surface superrepellent even to completely wetting liquids. *Science* **346**, 1096–1100.

[5] Lv, B., Lin, B., Sui, T., Zhang, J., Wang, L., Zhou, J., Zhao, P., Li, J., 2024. A 3-DOF spreading precision positional stage for ductile end-face fly-cutting of quartz glass. *Precision Engineering* **91**, 660–677.

[6] Wang, M., Zhong, W., Zeng, W., Gao, F., Yu, Y., Scott, P., Jiang, X., 2025. Towards high-speed on-machine measurement of freeform surfaces: a dynamic error calibration method. *Light: Advanced Manufacturing* **6**, 831–842.

[7] Vu, H.H., Nguyen, N.-T., Kashaninejad, N., 2023. Re-Entrant Microstructures for Robust Liquid Repellent Surfaces. *Advanced Materials Technologies* **8**. 2201-836.

[8] M., Bellussi, F.M., Morciano, M., Asinari, P., Fasano, M., 2023. Method for predicting the wettability of micro-structured surfaces by continuum phase-field modelling. *Methods*X **11**, 2215-0161.